

Cellular Uptake and Localization of Polymyxins in Renal Tubular Cells Using Rationally Designed Fluorescent Probes

Bo Yun,^{a,b} Mohammad A. K. Azad,^a Cameron J. Nowell,^c Roger L. Nation,^a Philip E. Thompson,^b Kade D. Roberts,^{a,b} Tony Velkov,^a Jian Li^a

Drug Delivery, Disposition and Dynamics,^a Medicinal Chemistry,^b and Drug Discovery Biology,^c Monash Institute of Pharmaceutical Sciences, Monash University, Melbourne, Victoria, Australia

Polymyxins are cyclic lipopeptide antibiotics that serve as a last line of defense against Gram-negative bacterial superbugs. However, the extensive accumulation of polymyxins in renal tubular cells can lead to nephrotoxicity, which is the major dose-limiting factor in clinical use. In order to gain further insights into the mechanism of polymyxin-induced nephrotoxicity, we have rationally designed novel fluorescent polymyxin probes to examine the localization of polymyxins in rat renal tubular (NRK-52E) cells. Our design strategy focused on incorporating a dansyl fluorophore at the hydrophobic centers of the polymyxin core structure. To this end, four novel regioselectively labeled monodansylated polymyxin B probes (MIPS-9541, MIPS-9542, MIPS-9543, and MIPS-9544) were designed, synthesized, and screened for their antimicrobial activities and apoptotic effects against rat kidney proximal tubular cells. On the basis of the assessment of antimicrobial activities, cellular uptake, and apoptotic effects on renal tubular cells, incorporation of a dansyl fluorophore at either position 6 or 7 (MIPS-9543 and MIPS-9544, respectively) of the polymyxin core structure appears to be an appropriate strategy for generating representative fluorescent polymyxin probes to be utilized in intracellular imaging and mechanistic studies. Furthermore, confocal imaging experiments utilizing these probes showed evidence of partial colocalization of the polymyxins with both the endoplasmic reticulum and mitochondria in rat renal tubular cells. Our results highlight the value of these new fluorescent polymyxin probes and provide further insights into the mechanism of polymyxin-induced nephrotoxicity.

Over the past 2 decades there has been a pronounced increase in the emergence of multidrug-resistant (MDR) Gram-negative bacterial superbugs, leading to serious infections that are resistant to almost all currently available antibiotics (1). The dire situation is perpetuated by a lack of novel antibiotics in the developmental pipeline, leaving the world in a vulnerable state against these life-threatening infections (1). This perfect storm has led to the revival of the polymyxin class of antibiotics, polymyxin B and polymyxin E (the latter of which is also known as colistin), as a last line of defense against MDR Gram-negative bacterial superbugs (2). Polymyxins are amphipathic cationic lipopeptides comprising hydrophobic and hydrophilic domains that are essential for their antibacterial activity (3). The general polymyxin structure consists of a cyclic heptapeptide ring with a linear tripeptide segment and an N-terminal fatty acyl tail (Table 1). Also present are five L- α,γ -diaminobutyric acid (Dab) residues, which contain primary amines that are positively charged at physiological pH (7.4), as well as two hydrophobic residues in positions 6 and 7 of the cyclic ring. The two polymyxins used clinically, polymyxin B and colistin, are differentiated by a single hydrophobic residue at position 6: D-leucine in colistin and D-phenylalanine in polymyxin B (3). Both polymyxins are products of fermentation, with each containing two major components (colistin A and B and polymyxin B₁ and B₂), which differ by one carbon at the fatty acyl tail (Table 1).

Despite their excellent antibacterial activity, the use of polymyxins has largely been limited by the associated toxicological effects. In particular, nephrotoxicity is the major dose-limiting factor for the clinical use of polymyxins, occurring in up to 60% of patients (1, 4–7). Polymyxin-induced nephrotoxicity is almost certainly linked to their complex renal handling (8–11). For both colistin and polymyxin B, only a very small fraction of the dose is

renally excreted (9, 11–13). The majority of the polymyxin molecules filtered at glomeruli undergo extensive renal reabsorption, leading to accumulation in tubular cells and the associated tubular damage (7–9, 12–14). Recent studies from our group have demonstrated that polymyxin-induced nephrotoxicity is related to oxidative stress and apoptosis in renal tubular cells and has induced DNA breakage and morphological changes in mitochondria (15). In a mouse nephrotoxicity model, increased expression of the biomarkers for mitochondrial and endoplasmic reticulum (ER) apoptosis pathways, including cytochrome *c*, apoptosis regulator BCL2-associated X protein (Bax), and the endoplasmic stress regulators 78-kDa glucose-regulated protein/binding immunoglobulin protein (Grp78/Bip) and activating transcription factor 6 (ATF6), is evident after colistin treatment (16).

To date there has been little information on the intracellular localization of polymyxins in renal tubular cells, which is important knowledge for understanding the mechanism of polymyxin-induced nephrotoxicity. Such studies require suitable fluorescent probes representative of the polymyxins to enable imaging of their uptake and localization within cells. The fluorescent probes pre-

Received 28 May 2015 Returned for modification 14 July 2015

Accepted 14 September 2015

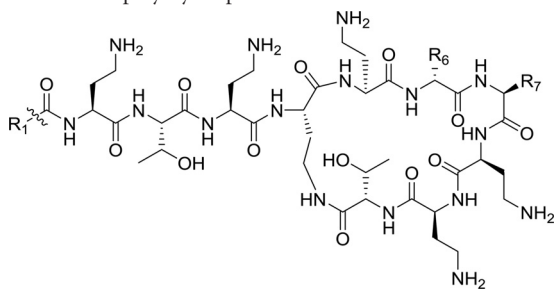
Accepted manuscript posted online 21 September 2015

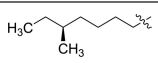
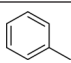
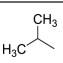
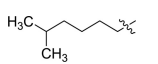
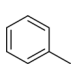
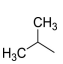
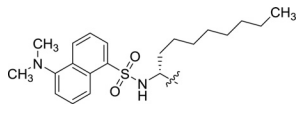
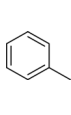
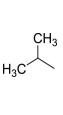
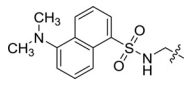
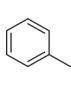
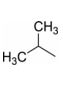
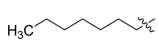
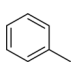
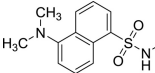
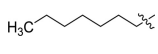
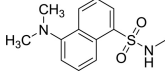
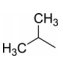
Citation Yun B, Azad MAK, Nowell CJ, Nation RL, Thompson PE, Roberts KD, Velkov T, Li J. 2015. Cellular uptake and localization of polymyxins in renal tubular cells using rationally designed fluorescent probes. *Antimicrob Agents Chemother* 59:7489–7496. doi:10.1128/AAC.01216-15.

Address correspondence to Tony Velkov, Tony.Velkov@monash.edu or Jian Li, colistin.polymyxin@gmail.com.

Copyright © 2015, American Society for Microbiology. All Rights Reserved.

TABLE 1 Structures of polymyxin B and the fluorescent polymyxin probes



Peptide	R ₁ (N terminus)	R ₆ (position 6)	R ₇ (position 7)
Polymyxin B ₁			
Polymyxin B ₂			
MIPS-9541			
MIPS-9542			
MIPS-9543			
MIPS-9544			

viously utilized (e.g., semisynthetic preparations of dansyl- and BODIPY-polymyxin B) for studying the mechanism of action, uptake, and localization of polymyxin (17–21) are not representative of the parent polymyxin (22–24). Our group recently reported the design and synthesis of a regioselectively monodansylated polymyxin B probe (MIPS-9541) for imaging uptake into bacterial cells (22). Our design approach provided a probe that possesses native antibacterial properties similar to those of the parent compound, polymyxin B. We have also used a similar probe design strategy to quantitatively measure the accumulation of polymyxins in single rat and human renal tubular cells (23). In the current study, we built on this probe design strategy to examine the localization of polymyxins in renal tubular cells. To be representative of the parent compound, polymyxin B, it is important that the designed probes retain both antimicrobial activity and apoptotic effects on kidney tubular cells. To this end, MIPS-9541, along with three new regioselectively monodansylated polymyxin B analogs (MIPS-9542, MIPS-9543, and MIPS-9544) (Table 1), were evaluated as polymyxin B probes for exploring the uptake and localization of polymyxins in renal tubular cells. For the first time, the intracellular colocalization of polymyxin B within the ER and mitochondria was visualized using fluorescence microscopy.

MATERIALS AND METHODS

General experimental. Polymyxin B (sulfate), colistin (sulfate), trifluoroacetic acid (TFA), diphenylphosphoryl azide (DPPA), dansylglycine, dansyl chloride, ethanedithiol (EDT), triisopropylsilane (TIPS), and hydrazine were purchased from Sigma-Aldrich (Sydney, NSW, Australia). Diisopropylethylamine (DIPEA) and piperidine were obtained from Aussep (Melbourne, Australia). 9-Fluorenylmethoxy carbonyl (Fmoc)-Dab(Boc)-OH was purchased from Try-lead Chem (China). Fmoc-Thr(tBu)-OH and Fmoc-Leu-OH were from Mimotopes (Melbourne, Australia). Fmoc-Dab(ivDde)-OH, Fmoc-D-Phe-OH, Fmoc-Dap-OH, Fmoc-D-Dap-OH, 1*H*-benzotriazolium-1-[bis(dimethylamino)methylene]-5-chloro-hexafluoro-phosphate-(1-),3-oxide (HCTU) (Chem-Impex International, Wood Dale, IL), and Thr(tBu)-TCP resin were from Intavis Bioanalytical Instruments (Germany). Diethyl ether, dichloromethane (DCM), dimethylformamide (DMF), methanol (MeOH), and acetonitrile were obtained from Merck (Melbourne, Australia). Fmoc-Dap(dansyl)-OH and Fmoc-D-Dap(dansyl)-OH were synthesized in accordance with a previously published method (17). Polymyxin B stock solutions were prepared with Milli-Q water (Millipore, North Ryde, NSW, Australia) and filtered using 0.22- μ m-pore-size syringe filters (Sartorius, Melbourne, Vic, Australia). Solutions were stored at 4°C for up to 1 month (24).

Peptides were purified by reverse-phase high-pressure liquid chromatography (RP-HPLC) on a Waters Prep liquid chromatography (LC) sys-

tem connected to a Waters 486 tuneable absorbance detector (214 nm), employing a Phenomenex Axia column {Luna C8(2); 250 by 50.0 mm [inside diameter (i.d.)], 100 Å, 10 µm}. Solvent A was 0.1% TFA–water, and solvent B was 0.1% TFA–acetonitrile. Peptides were eluted with a gradient of 0 to 60% solvent B over 60 min at a flow rate of 40 ml/min. The fractions collected were analyzed by analytical LC/mass spectrometry (MS) using a Shimadzu 2020 LCMS system incorporating a photodiode array detector (214 nm) coupled to an electrospray ionization source and a single quadrupole mass analyzer. Solvent A was 0.05% TFA–water, and solvent B was 0.05% TFA–acetonitrile. A Phenomenex column [Luna C8(2), 100 by 2.0 mm (i.d.)] was used for RP-HPLC, eluting with a gradient of 0 to 60% solvent B over 10 min at a flow rate of 0.2 ml/min. Mass spectra were acquired in positive ion mode with a scan range of 200 to 2,000 *m/z*.

Synthesis of fluorescently labeled polymyxin probes. (i) MIPS-9541 (TFA salt). The synthesis of MIPS-9541 (formerly identified as FADDI-043) has been previously described by our group (22). In the present study, we used an optimized synthetic procedure, which is described in detail here. Synthesis of the protected linear peptide was conducted on a Protein Technologies Prelude automated peptide synthesizer using standard Fmoc solid-phase peptide chemistry. Specifically, synthesis was undertaken using TCP-resin preloaded with Fmoc-Thr(tBu)-OH (0.1-mmol scale). Coupling of the Fmoc-amino acids was performed using the default instrument protocol: 3 molar equivalents (relative to the level of resin loading) of the Fmoc amino acid and HCTU in DMF with activation *in situ*, using 6 molar equivalents of DIPEA. This was carried out for 50 min at room temperature. The N-terminal dansyl group was coupled using 3 molar equivalents (relative to the level of resin loading) of dansyl chloride in DMF in the presence of 6 molar equivalents of DIPEA. Fmoc deprotection was conducted using the default instrument protocol: 20% piperidine in DMF (once for 5 min, once for 10 min) at room temperature. Removal of the ivDde protecting group was achieved with 3% hydrazine in DMF (4 times for 15 min each time). The protected linear peptide was then cleaved from the resin by treating the resin with 20% hexafluoroisopropanol (HFIP) in DCM (once for 30 min, once for 5 min). This solution was concentrated *in vacuo* to give the crude protected linear peptide. The protected linear peptide was dissolved in DMF (5 ml) to which DIPEA (0.6 mmol, 104 µl [6 molar equivalents relative to the level of loading of the resin]) and DPPA (0.3 mmol, 0.65 µl [3 molar equivalents relative to the level of loading of the resin]) were added. The solution was stirred at room temperature for 5 h. The reaction solution was then concentrated under vacuum overnight to give the crude protected cyclic peptide. The resulting residue was taken up in a solution of 2.5% EDT, 5% TIPS in TFA and stirred at room temperature for 2 h. To this solution, 40 ml of diethyl ether was added. The resulting precipitate was collected by centrifugation, washed twice with diethyl ether (40 ml), and then air dried in a fume hood to give the crude cyclic peptide as a pale yellow solid. The resulting solid was taken up in Milli-Q water (5 ml) and desalted using a Vari-Pure IPE SAX column. The solution containing the crude cyclic peptide was subjected to RP-HPLC purification, and the collected fractions were analyzed by LC-MS, as described above. The combined fractions were freeze-dried for 2 days to give the MIPS-9541 TFA salt as a pale yellow solid in a yield of 57.0 mg. The purity was >95%, as determined by RP-HPLC at 214 nm. The compound was confirmed to have the correct molecular weight by electrospray ionization (ESI)-MS analysis: *m/z* (monoisotopic) calculated: C₇₁H₁₁₆N₁₉O₁₆S [M + H]⁺ 1,523.86, [M + 2H]²⁺ 762.43, [M + 3H]³⁺ 508.62; observed: [M + H]⁺ 1,523.20, [M + 2H]²⁺ 762.45, [M + 3H]³⁺ 508.70.

MIPS-9542 (TFA salt). MIPS-9542 was synthesized as described above for MIPS-9541 to give the MIPS-9542 TFA salt as a pale yellow solid in a yield of 65.2 mg with >95% purity, estimated by RP-HPLC at 214 nm. The molecular weight was confirmed by ESI-MS analysis; *m/z* (monoisotopic) calculated: C₆₁H₉₆N₁₈O₁₅S [M + H]⁺ 1,353.70, [M + 2H]²⁺ 677.35, [M + 3H]³⁺ 451.90; observed: [M + H]⁺ 1,353.70, [M + 2H]²⁺ 677.85, [M + 3H]³⁺ 452.30.

MIPS-9543 (TFA salt). MIPS-9543 was synthesized as described above for MIPS-9541 to give the MIPS-9543 TFA salt as a pale yellow solid in a yield of 53.9 mg with >95% purity, estimated by RP-HPLC at 214 nm. The molecular weight was confirmed by ESI-MS analysis: *m/z* (monoisotopic) calculated: C₆₄H₁₀₂N₁₈O₁₅S [M + H]⁺ 1,395.75, [M + 2H]²⁺ 698.37, [M + 3H]³⁺ 465.92; observed: [M + H]⁺ 1,395.85, [M + 2H]²⁺ 698.85, [M + 3H]³⁺ 466.30.

MIPS-9544 (TFA salt). MIPS-9544 was synthesized as described above for MIPS-9541 to give the MIPS-9544 TFA salt as a pale yellow solid in a yield of 62.0 mg with >95% purity, estimated by RP-HPLC. The molecular weight was confirmed by ESI-MS analysis: *m/z* (monoisotopic) calculated: C₆₁H₁₀₄N₁₈O₁₅S [M + H]⁺ 1,361.76, [M + 2H]²⁺ 681.38, [M + 3H]³⁺ 454.59; observed: [M + H]⁺ 1,361.95, [M + 2H]²⁺ 681.90, [M + 3H]³⁺ 455.00.

Determination of MICs. MICs for *Pseudomonas aeruginosa*, *Klebsiella pneumoniae*, and *Acinetobacter baumannii* strains were determined by the broth microdilution method (26). Experiments were conducted in 96-well polypropylene microtiter plates with all dilutions using cation-adjusted Mueller-Hinton broth (CaMHB). The bacterial suspension (100 µl containing ~10⁶ CFU per ml) was added to the wells in the presence of increasing concentrations of polymyxins (0 to 128 mg/liter).

Culture of rat kidney tubular cells. Rat kidney proximal tubular cells (NRK-52E cells; ATCC) were employed for intracellular localization and apoptosis studies. Dulbecco's modified Eagle's medium (DMEM) supplemented with 10% fetal bovine serum (FBS) was used. The growth medium components were purchased from Invitrogen (Life Technologies, Victoria, Australia). NRK-52E cells (0.5 × 10⁵ cells/ml) were seeded in 24-well plates, 12-well plates, or 8-well chamber slides in the supplemented DMEM at 37°C in a humidified atmosphere containing 5% CO₂ until they were 60 to 70% confluent. The probe incubations were conducted in DMEM supplemented with 0.1% FBS.

Apoptosis assay. Apoptosis studies were conducted using an Alexa Fluor 680-annexin V/Dead Cell Apoptosis kit (Invitrogen). NRK-52E cells were cultured in 12-well plates until they were ~60 to 70% confluent and incubated with or without the fluorescent polymyxin probes (50 and 250 µM) or the positive control, polymyxin B (2 mM), for 16 h. Following incubation, the cells in the plates were washed with phosphate-buffered saline (PBS). The supernatant was discarded, and the cells were detached from the plates using 200 µl of trypsin-EDTA solution (0.05%) for 5 min at 37°C. Trypsin was inactivated with addition of 0.5 ml of DMEM. The cell suspension was washed three times by centrifugation (450 × g, 5 min), and the supernatant was discarded. Following the third wash, cell pellets were resuspended in 100 µl of ice-cold 1 × annexin-binding buffer. Five microliters of Alexa Fluor 680-conjugated annexin V and 1 µl of propidium iodide (PI; 100 µg/ml) were added to the suspension, and the cells were incubated in the dark at room temperature. After 15 min, 0.4 ml of ice-cold 1 × annexin-binding buffer was added to the cells, and the induction of apoptosis was monitored by fluorescence-activated cell sorting (FACS; MoFlo Astrios). Fluorescence emission was measured using an excitation wavelength of 488 nm and an emission wavelength of 575 nm for PI and an excitation wavelength of 680 nm and an emission wavelength of 700 nm for Alexa Fluor 680-conjugated annexin V. Annexin V-positive and PI-negative cells and annexin V-positive and PI-positive cells were labeled as early and late apoptotic cells, respectively. The percentage of apoptotic cells in the total number of cells was designated the apoptotic index (AI). All experiments were conducted in three independent replicates, and data are presented as the mean ± standard deviation (SD). Significance testing was performed using two-way analysis of variance (ANOVA) and Tukey's test for multiple comparisons, with significance being considered when the *P* value was <0.05.

Concentration-dependent uptake of the fluorescent probes using CLSM. Confocal laser scanning microscopy (CLSM) was performed using a Leica Microsystems TCS SP8 CLSM (Wetzlar, Germany) with a ×63 PlanApo (numerical aperture, 1.4) oil immersion objective. The filters were chosen to avoid cross detection between the probes, and no auto-

TABLE 2 MICs of polymyxin B and fluorescent probes against polymyxin-susceptible Gram-negative strains

Bacterial species and strain	MIC ($\mu\text{g/ml}$)				
	Polymyxin B	MIPS-9541	MIPS-9542	MIPS-9543	MIPS-9544
<i>P. aeruginosa</i>					
ATCC 27853	1	4	2	2	1
FADDI-PA022	1	4	2	2	2
FADDI-PA025	1	4	2	4	4
<i>K. pneumoniae</i>					
ATCC 13883	1	8	2	2	2
FADDI-KP032	<0.125	8	ND ^a	1	1
<i>A. baumannii</i>					
ATCC 19606	1	4	4	2	4
ATCC 17978	1	4	1	2	4
FADDI-AB034	0.5	8	2	2	2

^a ND, not determined.

fluorescence was detected with the collection parameters. For the dansyl group, samples were scanned using an excitation wavelength of 405 nm and an emission wavelength of 470 to 560 nm. Concentration-dependent uptake of the polymyxin probes in NRK-52E cells was examined using cells cultured to ~60 to 70% confluence in 24-well plates on coverslips and incubated with or without the desired probe derivative (final concentrations, 25, 50, 100, 200, 500, and 1,000 μM ; 4 h). After incubation, the cells were washed with PBS, followed by fixation in 4% paraformaldehyde for 15 min and washing of the cells twice with PBS. The slides were then dried and fixed onto glass slides using Mowiol (Calbiochem) before imaging. The images were processed and analyzed using the open-source image analysis software ImageJ (<http://imagej.nih.gov/ij/>) (27). The concentration of each probe required to reach 50% of maximal uptake (50% effective concentration [EC₅₀]) was determined by sampling of 20 individual cells and calculated using the unweighted nonlinear least-squares regression model in GraphPad Prism software (v6.0; GraphPad Software, San Diego, CA, USA). All experiments were conducted in three independent replicates, and data are presented as the mean \pm SD.

Studies of fluorescent probe localization. Endoplasmic reticulum (ER) Tracker Red, purchased from Invitrogen (Life Technologies), was reconstituted in 110 μl of dimethyl sulfoxide to yield a 1 mM stock solution, which was diluted with Dulbecco's modified Eagle's medium (Life Technologies) to a final working concentration of 1 μM . LysoTracker Deep Red, purchased from Invitrogen (Life Technologies), was diluted to a working concentration of 50 nM. MitoTracker Red, purchased from Invitrogen (Life Technologies), was diluted to a working concentration of 200 nM. NRK-52E cells were grown to ~60 to 70% confluence in 8-well chamber slides and incubated with or without MIPS-9541 (at 25 μM for 4 h) or with or without MIPS-9542, MIPS-9543, or MIPS-9544 (each at 200 μM for 4 h). Cells were then stained by addition of 250 μl prewarmed ER-Tracker Red, LysoTracker Deep Red, or MitoTracker Red working solution and incubated for 20 min (or 30 min for MitoTracker Red) at 37°C. After incubation, the medium was changed to phenol red-free DMEM and the cells were imaged directly with the CLSM.

RESULTS

Antibacterial activity of the probes. The antibacterial activity of the probes against a panel of polymyxin-susceptible ATCC strains and clinical isolates of *P. aeruginosa*, *K. pneumoniae*, and *A. baumannii* was assessed (Table 2). All four probes were active against the examined bacterial strains, with most MICs being 2- to 8-fold higher than the MIC of polymyxin B.

Apoptotic effects of the probes. Given that the clinically used polymyxins can induce apoptosis in kidney proximal tubular cells, we employed an *in vitro* cell-based apoptosis assay to investigate

the apoptotic effects of the probes (15). Similar to polymyxin B, all the probes, with the exception of MIPS-9542, induced various degrees of apoptosis in NRK-52E cells (Fig. 1). MIPS-9541 was the most cytotoxic, with an AI of ~99.9% at 50 μM . MIPS-9543 (AI = ~47.4%) and MIPS-9544 (AI = ~32.0%) demonstrated lower apoptotic indices at 250 μM and no significant apoptosis at 50 μM relative to that for the untreated control. MIPS-9542 showed no significant apoptosis relative to that for the untreated control at both 50 μM and 250 μM .

Uptake and subcellular localization of the probes in renal tubular cells. NRK-52E cells treated with different concentrations of each probe showed various degrees of cellular uptake, as gauged by the intensity of fluorescence observed in the confocal microscopy images of the treated cells (Fig. 2). Cells treated with MIPS-9541 demonstrated the highest fluorescence intensity relative to that for cells treated with the other probes at 500 μM . Significant fluorescence was also observed for cells treated with MIPS-9541 at 200 μM . In contrast, NRK-52E cells treated with MIPS-9542 at either 500 μM or 1,000 μM showed no significant fluorescence. Cells treated with MIPS-9543 and MIPS-9544 at 500 μM but not at 250 μM showed significant fluorescence. Plotting of the emission intensity per cell as a function of the probe concentration (Fig. 3) showed a concentration-dependent relationship for MIPS-9541, MIPS-9543, and MIPS-9544. The confocal images revealed that the probes distributed mainly in the cytoplasm and around the nucleus (Fig. 2). Bright fluorescent spots were also observed inside the nuclei of cells treated with MIPS-9541, MIPS-9543, and MIPS-9544 (Fig. 2). Initial studies conducted with the lysosome-selective dye LysoTracker Deep Red indicated a lack of colocalization of the probes within lysosomes (Fig. 4). However, subcellular imaging studies with the ER-selective dye ER-Tracker Red and mitochondrion-selective dye MitoTracker Red in live cells showed that MIPS-9541, MIPS-9543, and MIPS-9544 demonstrated partial colocalization with both the ER and mitochondria in NRK-52E cells.

DISCUSSION

Nephrotoxicity is the major dose-limiting adverse effect of polymyxins for achieving optimal plasma concentrations in patients (6, 9, 28). The primary goal of this study was to investigate the localization of polymyxins in renal tubular cells using rationally

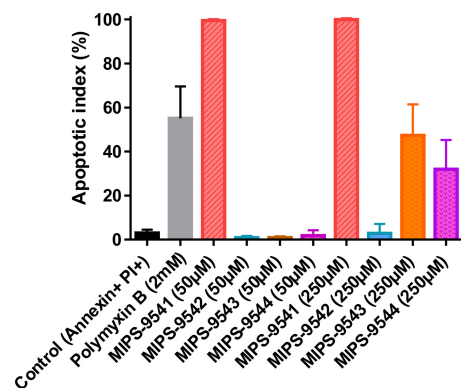


FIG 1 Apoptotic indices (mean \pm SD, $n = 3$) of NRK-52E cells incubated with 50 or 250 μM MIPS-9541, MIPS-9542, MIPS-9543, or MIPS-9544 or 2 mM polymyxin B for 16 h. Two-way ANOVA was performed for analysis of significance ($\alpha = 0.05$).

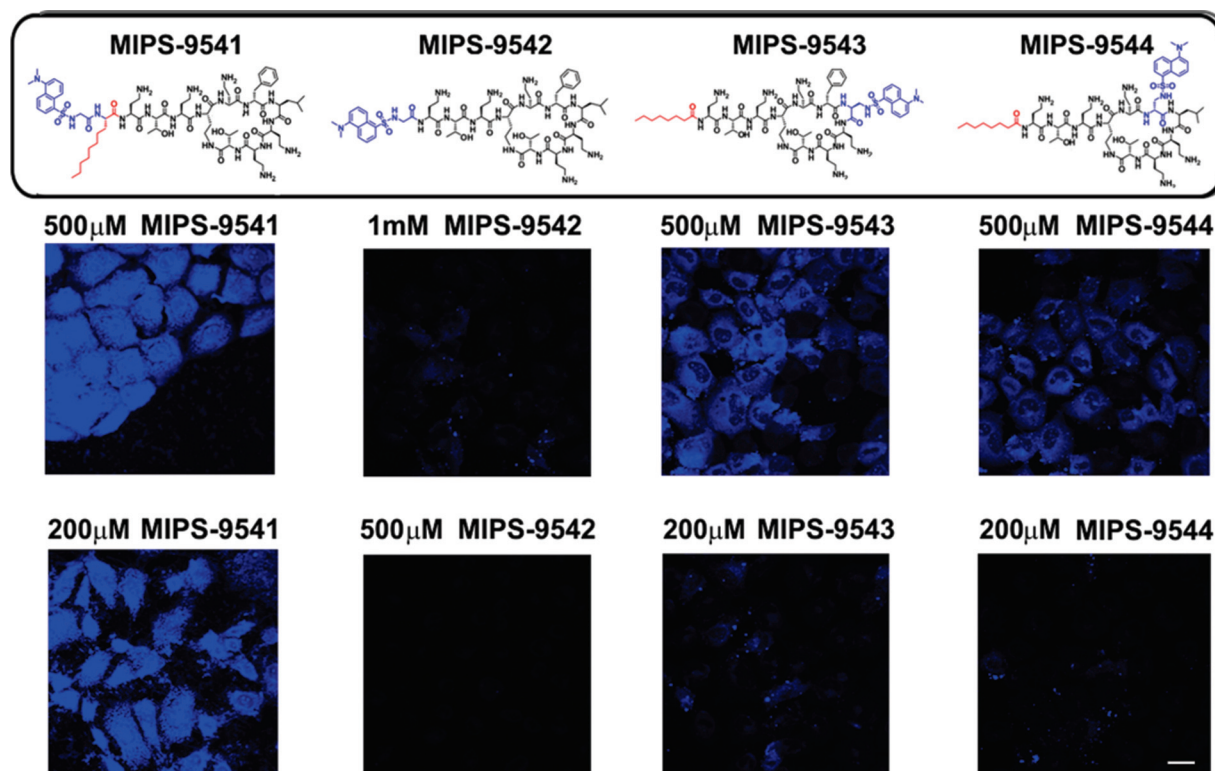


FIG 2 Confocal microscopy images of rat kidney tubular NRK-52E cells treated with MIPS-9541, MIPS-9542, MIPS-9543, and MIPS-9544 at the indicated concentrations for 4 h. The chemical structure of each probe is shown at the top, with the fluorophore modification being shown in blue. Bar = 20 μm .

designed fluorescent probes that have pharmacological and toxicological activity representative of that of the parent compound, polymyxin B (2). A lack of native antibacterial activity is the major shortcoming of the commercially available dansyl-polymyxin B and BODIPY-polymyxin B probes that have been utilized in the past (18–21). Our group has previously highlighted the pitfalls of directly coupling fluorescent groups, such as dansyl, onto the Dab side chains, such as those which occur with the semisynthetic preparations of dansyl-polymyxin B (22, 24, 25). Accordingly, there is little value in using these semisynthetic preparations as probes for imaging polymyxin localization in renal tubular cells. Here we designed and synthesized a series of regioselectively mod-

ified monodansylated polymyxin B probes with the previously reported polymyxin B-lipid A interaction principles in mind in order to maintain the native antibacterial activity and toxicity profile of the parent polymyxin B. The probes were designed by regioselectively modifying the hydrophobic centers within the polymyxin scaffold at the N-terminal fatty acyl tail or the position 6 or 7 residue. It was hypothesized that the addition of a hydrophobic fluorophore to these regions would have less impact than would incorporation at other more hydrophilic regions of the molecule (Table 1). To this end, the hydrophobic dansyl group was utilized as the fluorophore. The comparatively small size of the dansyl group relative to the size of other fluorophores also helped reduce the likelihood of negative steric effects on the pharmacophore of polymyxins (3). We have previously reported the design and synthesis strategy for MIPS-9541 (22). In this probe, the fatty acyl group of polymyxin B was substituted with L-octylglycine (C_8), which served to mimic the eight-carbon fatty acyl chain of polymyxin B₁ with the N^α -amino group, providing a point of attachment for the dansyl group (22). For MIPS-9542, the dansyl fluorophore was substituted *in lieu* of the N-terminal fatty acyl tail, as it has previously been demonstrated that a variety of hydrophobic groups are well tolerated at this position and act as mimics of the N-terminal saturated alkyl fatty acyl chains of polymyxins B₁ and B₂ (3). For MIPS-9543 and MIPS-9544, the hydrophobic D-Phe and D-Leu residues at positions 6 and 7 of the polymyxin core, respectively, were substituted with a Dap(dansyl) moiety to evaluate substitutions at these hydrophobic centers. We have previously shown that the amino acid residues at positions 6 and 7 can be readily substituted with structurally diverse hydrophobic

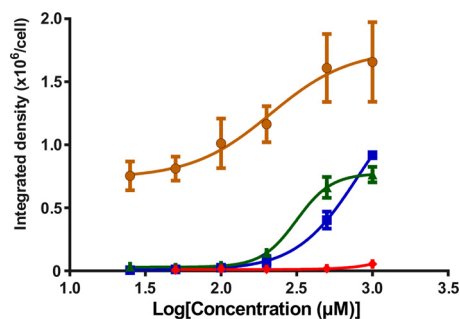


FIG 3 Plot of the integrated density of each probe per NRK-52E cell ($n = 20$ cells) from the confocal microscopy imaging data (as exemplified in Fig. 2) against the log concentration (in micromolar). The solid lines represent the best fit to a nonlinear dose-response model. ●, MIPS-9541; ◆, MIPS-9542; ▲, MIPS-9543; ■, MIPS-9544. Data are presented as mean \pm SD.

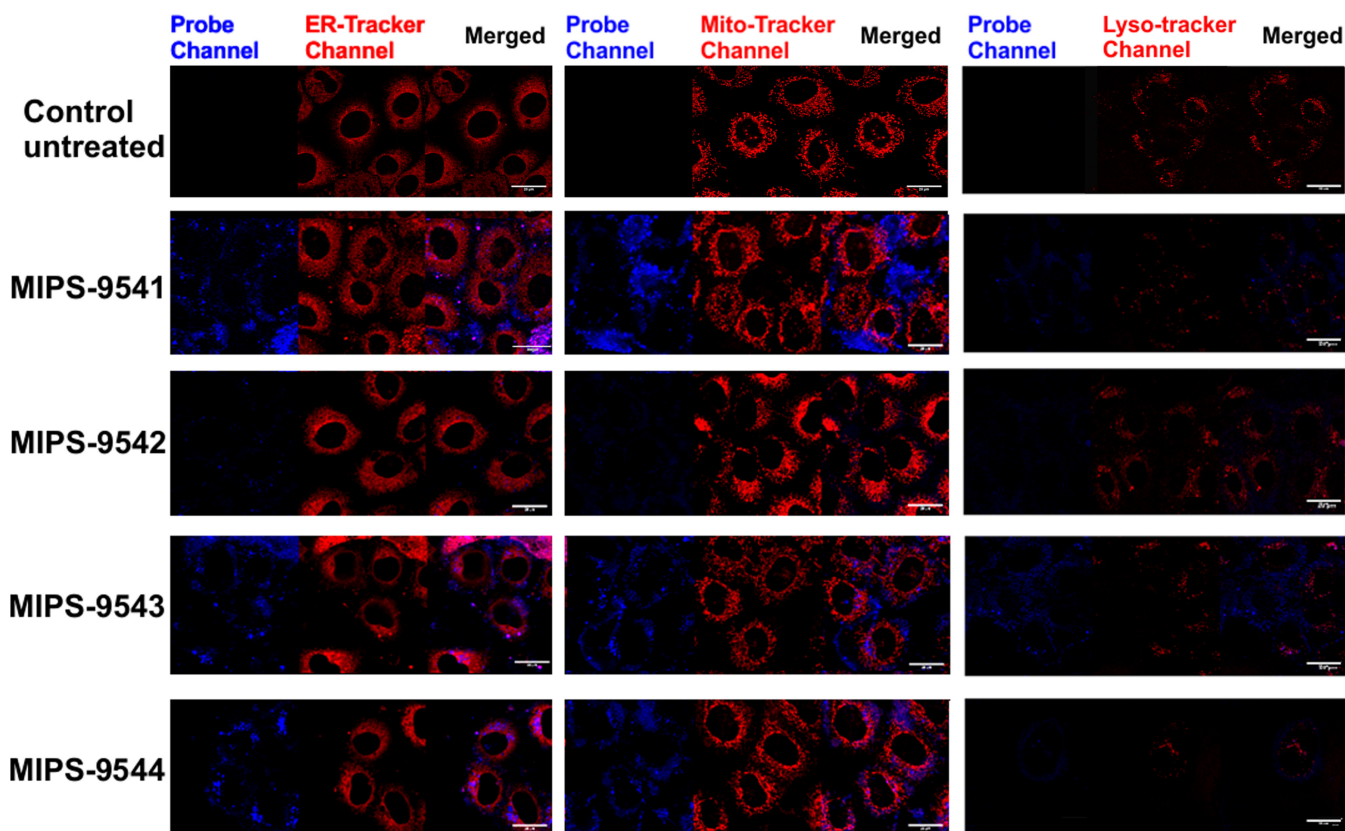


FIG 4 Subcellular imaging of NRK-52E cells treated with ER-Tracker Red (left), MitoTracker Red (middle), or LysoTracker Deep Red (right) and the polymyxin probes MIPS-9541 (25 μ M), MIPS-9542 (200 μ M), MIPS-9543 (200 μ M), and MIPS-9544 (200 μ M) for 4 h at 37°C. Bars = 20 μ m.

amino acid residues (e.g., biphenylalanine) without significantly affecting the antibacterial activity of the compound (29).

Our design strategy provided probes that had antimicrobial activity similar to that of polymyxin B against the Gram-negative bacterial strains screened (Table 2). MIPS-9541, in which the N-terminal fatty acyl chain was substituted with the dansyl-octylglycine group, was slightly less active (MICs, 4 to 8 μ g/ml) than MIPS-9542, MIPS-9543, and MIPS-9544, all of which had MICs in the range of 1 to 4 μ g/ml. These results suggest that incorporation of the dansyl fluorophore only at the N terminus (MIPS-9542) or at position 6 (MIPS-9543) or 7 (MIPS-9544) of the polymyxin core afforded better surrogates for the native polymyxins with respect to the antimicrobial activity. Incorporation of both the dansyl fluorophore and a C₈ fatty acyl chain (octylglycine) at the N terminus (MIPS-9541) does not appear to be as favorable for the antimicrobial activity. This may be due to unfavorable steric effects or conformational changes preventing the peptide from optimally binding to lipid A to initiate its antimicrobial effect (3). Antimicrobial activity comparable to that of the native polymyxin B was obtained with our probe design strategy focusing on the modification of only the hydrophobic centers of the polymyxin core; this strategy further highlights the importance of not modifying the hydrophilic Dab residues of the polymyxin core (22, 24). To further assess the polymyxin likeness of the probes, an *in vitro* cell-based assay was conducted to examine their potential apoptotic effects on renal tubular cells, with apoptotic cell death being one of the presenting pathological changes in polymyxin-

induced nephrotoxicity (15, 30). In the present study, 2 mM polymyxin B was employed as a positive control to show ~50% cells in apoptosis. Interestingly, the apoptotic indices for the four probes varied considerably. MIPS-9541 demonstrated a markedly higher apoptotic index (~99.9% at 50 μ M) than polymyxin B (~55% at 2 mM). However, for probes MIPS-9542, MIPS-9543, and MIPS-9544, no significant apoptotic effect was observed at 50 μ M (Fig. 1). The situation was different at 250 μ M, where MIPS-9543 (apoptotic index, ~50%) and MIPS-9544 (apoptotic index, ~35%) showed marked increases in the degree of apoptosis observed. This was not the case for MIPS-9542, which showed no significant increase in the degree of apoptosis even at 250 μ M.

Confocal fluorescence microscopy experiments demonstrated the cellular uptake of all four probes by the renal tubular cells (Fig. 2). MIPS-9541, in which both the octylglycine and the dansyl fluorophore are present at the N terminus, showed the highest uptake, with significant intracellular fluorescence being observed at both 500 and 200 μ M. MIPS-9543 and MIPS-9544 displayed similar levels of intracellular fluorescence (Fig. 2). Interestingly, MIPS-9542, which contains the native polymyxin B scaffold selectively modified by substitution of the N-terminal fatty acyl chain with the dansyl fluorophore, displayed the lowest uptake by NRK-52E cells (Fig. 2). For MIPS-9541, MIPS-9543, and MIPS-9544, uptake by NRK-52E cells appeared to be concentration dependent, as revealed by plotting of the emission intensity per cell as a function of the probe concentration (Fig. 3). Taken together, these results suggest that the chemical nature (structure) of the fatty acyl group

presented at the N-terminal region of the polymyxin B core is a factor in the promotion of polymyxin uptake by the renal tubular cells *in vitro*. However, further work needs to be undertaken to determine whether this is translated to renal tubular cells *in vivo*. The degree of cellular uptake observed for the respective probes in the fluorescence imaging experiments correlated well with the apoptotic indices observed for the four probes (Fig. 1 and 3). MIPS-9451 had the highest degree of cellular uptake and the highest apoptotic index, while MIPS-9542 had a low degree of cellular uptake and displayed no significant apoptosis even at 1,000 μ M. These results add further support to previous experimental findings that point to the accumulation of the polymyxins in renal tubular cells as being a predisposing factor for polymyxin-induced nephrotoxicity (14, 23). Taking into consideration the degree of cellular uptake along with the antimicrobial activity and apoptotic index for the four probes, MIPS-9543 and MIPS-9544, in which the dansyl fluorophore is incorporated at either position 7 or 6 of the polymyxin core, appear to be the best candidates for use as a fluorescent probe for polymyxin B and colistin.

The subcellular imaging experiments revealed that all of the probes except MIPS-9542 partially colocalized to the ER and mitochondria in NRK-52E cells, suggesting that accumulation in these organelles may be an inducer of the cellular toxicity. Mitochondria and ER form structural and functional networks essential for maintenance of cellular homeostasis and determine the cell fate under various pathophysiological conditions, including oxidative stress (31). This correlates with the current literature evidence that both the ER and mitochondrial pathways are involved in polymyxin-induced nephrotoxicity (16, 30, 32). Recently, it was reported that activation of the death receptor and mitochondrial pathways is involved in polymyxin-induced apoptosis in NRK-52E cells (15, 30). DNA fragmentation resulting from the activation of caspase-3, -8, and -9, as well as significant morphological damage to the mitochondria, was observed in NRK-52E cells after polymyxin B treatment (1.0 and 2.0 mM for 24 h) (31). Furthermore, in a mouse nephrotoxicity model, Dai et al. observed significant upregulation and downregulation of biomarkers for the mitochondrial pathway (upregulation of cytochrome *c* and Bax, as well as downregulation of Bcl-2) and the ER pathway (upregulation of Grp78/Bap, ATF6, GADD153/CHOP, and caspase-12) after a 7-day treatment with colistin (16). Pathological changes were also observed in the mitochondria of renal tubular cells from colistin-treated mice, where the organelles appeared to be swollen and ruptured (16). In addition, our results using the probes revealed that lysosomal colocalization was not evident at the time point examined (Fig. 4). Further experimental work is required to investigate the trafficking and recycling of polymyxins in renal tubular cells.

Conclusions. In this study, we rationally designed and synthesized novel fluorescent probes for exploring the uptake and localization of polymyxins in rat kidney cells. For the first time, we were able to provide visual evidence of the intracellular disposition of polymyxins in live renal tubular cells. The findings presented here provide further valuable insights into the possible mechanism of polymyxin-induced nephrotoxicity, which is crucial for optimizing their use in the clinic and for designing novel safer polymyxins.

ACKNOWLEDGMENTS

J.L., T.V., R.L.N., P.E.T., and K.D.R. are supported by a research grant from the National Institute of Allergy and Infectious Diseases of the Na-

tional Institutes of Health (R01 AI098771). J.L. is an Australian NHMRC Senior Research Fellow. T.V. is an Australian NHMRC Industry Career Development Research fellow.

The content is solely the responsibility of the authors and does not necessarily represent the official views of the National Institute of Allergy and Infectious Diseases or the National Institutes of Health.

REFERENCES

- Boucher HW, Talbot GH, Benjamin DK, Jr, Bradley J, Guidos RJ, Jones RN, Murray BE, Bonomo RA, Gilbert D. 2013. 10 × '20 progress—development of new drugs active against Gram-negative bacilli: an update from the Infectious Diseases Society of America. *Clin Infect Dis* 56:1685–1694. <http://dx.doi.org/10.1093/cid/cit152>.
- Velkov T, Roberts KD, Nation RL, Thompson PE, Li J. 2013. Pharmacology of polymyxins: new insights into an 'old' class of antibiotics. *Future Microbiol* 8:711–724. <http://dx.doi.org/10.2217/fmb.13.39>.
- Velkov T, Thompson PE, Nation RL, Li J. 2010. Structure-activity relationships of polymyxin antibiotics. *J Med Microbiol* 53:1898–1916. <http://dx.doi.org/10.1021/jm900999h>.
- Landman D, Georgescu C, Martin DA, Quale J. 2008. Polymyxins revisited. *Clin Microbiol Rev* 21:449–465. <http://dx.doi.org/10.1128/CMR.00006-08>.
- Akajagbor DS, Wilson SL, Shere-Wolfe KD, Dakum P, Charurat ME, Gilliam BL. 2013. Higher incidence of acute kidney injury with intravenous colistimethate sodium compared with polymyxin B in critically ill patients at a tertiary care medical center. *Clin Infect Dis* 57:1300–1303. <http://dx.doi.org/10.1093/cid/cit453>.
- Hartzell JD, Neff R, Ake J, Howard R, Olson S, Paolino K, Vishnepolsky M, Weintrob A, Wortmann G. 2009. Nephrotoxicity associated with intravenous colistin (colistimethate sodium) treatment at a tertiary care medical center. *Clin Infect Dis* 48:1724–1728. <http://dx.doi.org/10.1086/599225>.
- Kubin CJ, Ellman TM, Phadke V, Haynes LJ, Calfee DP, Yin MT. 2012. Incidence and predictors of acute kidney injury associated with intravenous polymyxin B therapy. *J Infect* 65:80–87. <http://dx.doi.org/10.1016/j.jinf.2012.01.015>.
- Abdelraouf K, Braggs KH, Yin T, Truong LD, Hu M, Tam VH. 2012. Characterization of polymyxin B-induced nephrotoxicity: implications for dosing regimen design. *Antimicrob Agents Chemother* 56:4625–4629. <http://dx.doi.org/10.1128/AAC.00280-12>.
- Sandri AM, Landersdorfer CB, Jacob J, Boniatti MM, Dalarosa MG, Falci DR, Behle TF, Bordinhao RC, Wang J, Forrest A, Nation RL, Li J, Zavascki AP. 2013. Population pharmacokinetics of intravenous polymyxin B in critically ill patients: implications for selection of dosage regimens. *Clin Infect Dis* 57:524–531. <http://dx.doi.org/10.1093/cid/cit334>.
- Ma Z, Wang J, Nation RL, Li J, Turnidge JD, Coulthard K, Milne RW. 2009. Renal disposition of colistin in the isolated perfused rat kidney. *Antimicrob Agents Chemother* 53:2857–2864. <http://dx.doi.org/10.1128/AAC.00030-09>.
- Li J, Milne RW, Nation RL, Turnidge JD, Smeaton TC, Coulthard K. 2003. Use of high-performance liquid chromatography to study the pharmacokinetics of colistin sulfate in rats following intravenous administration. *Antimicrob Agents Chemother* 47:1766–1770. <http://dx.doi.org/10.1128/AAC.47.5.1766-1770.2003>.
- Zavascki AP, Goldani LZ, Li J, Nation RL. 2007. Polymyxin B for the treatment of multidrug-resistant pathogens: a critical review. *J Antimicrob Chemother* 60:1206–1215. <http://dx.doi.org/10.1093/jac/dkm357>.
- Li J, Milne RW, Nation RL, Turnidge JD, Coulthard K. 2003. Stability of colistin and colistin methanesulfonate in aqueous media and plasma as determined by high-performance liquid chromatography. *Antimicrob Agents Chemother* 47:1364–1370. <http://dx.doi.org/10.1128/AAC.47.4.1364-1370.2003>.
- Yun B, Azad MA, Wang J, Nation RL, Thompson PE, Roberts KD, Velkov T, Li J. 2015. Imaging the distribution of polymyxins in the kidney. *J Antimicrob Chemother* 70:827–829. <http://dx.doi.org/10.1093/jac/dku441>.
- Azad MA, Finin BA, Poudyal A, Davis K, Li J, Hill PA, Nation RL, Velkov T. 2013. Polymyxin B induces apoptosis in kidney proximal tubular cells. *Antimicrob Agents Chemother* 57:4329–4335. <http://dx.doi.org/10.1128/AAC.02587-12>.
- Dai C, Li J, Tang S, Li J, Xiao X. 2014. Colistin-induced nephrotoxicity in mice involves the mitochondria, death receptor, and endoplasmic re-

- ticulum pathways. *Antimicrob Agents Chemother* 58:4075–4085. <http://dx.doi.org/10.1128/AAC.00070-14>.
17. Fattori D, Urbani A, Brunetti M, Ingenito R, Pessi A, Prendergast K, Narjes F, Matassa VG, Francesco RD, Steinkuhler C. 2000. Probing the active site of the hepatitis C virus serine protease by fluorescence resonance energy transfer. *J Biol Chem* 275:15106–15113. <http://dx.doi.org/10.1074/jbc.275.20.15106>.
 18. Abdelraouf K, Chang KT, Yin T, Hu M, Tam VH. 2014. Uptake of polymyxin B into renal cells. *Antimicrob Agents Chemother* 58:4200–4202. <http://dx.doi.org/10.1128/AAC.02557-14>.
 19. Moore RA, Bates NC, Hancock RE. 1986. Interaction of polycationic antibiotics with *Pseudomonas aeruginosa* lipopolysaccharide and lipid A studied by using dansyl-polymyxin. *Antimicrob Agents Chemother* 29:496–500. <http://dx.doi.org/10.1128/AAC.29.3.496>.
 20. Schindler PRG, Teuber M. 1975. Action of polymyxin B on bacterial membranes: morphological changes in the cytoplasm and in the outer membrane of *Salmonella typhimurium* and *Escherichia coli* B. *Antimicrob Agents Chemother* 8:95–104. <http://dx.doi.org/10.1128/AAC.8.1.95>.
 21. Benincasa M, Pacor S, Gennaro R, Scocchi M. 2009. Rapid and reliable detection of antimicrobial peptide penetration into Gram-negative bacteria based on fluorescence quenching. *Antimicrob Agents Chemother* 53:3501–3504. <http://dx.doi.org/10.1128/AAC.01620-08>.
 22. Deris ZZ, Swarbrick JD, Roberts KD, Azad MA, Akter J, Horne AS, Nation RL, Rogers KL, Thompson PE, Velkov T, Li J. 2014. Probing the penetration of antimicrobial polymyxin lipopeptides into Gram-negative bacteria. *Bioconjug Chem* 25:750–760. <http://dx.doi.org/10.1021/bc500094d>.
 23. Azad MA, Roberts KD, Yu HH, Schofield AV, James SA, Howard DL, Nation RL, Rogers KL, De-Jonge MD, Thompson PE, Fu J, Velkov T, Li J. 2015. Significant accumulation of polymyxin in single renal tubular cells: a medicinal chemistry and triple correlative microscopy approach. *Anal Chem* 87:1590–1595. <http://dx.doi.org/10.1021/ac504516k>.
 24. Soon RL, Velkov T, Chiu F, Thompson PE, Kancharla R, Roberts K, Larson I, Nation RL, Li J. 2011. Design, synthesis, and evaluation of a new fluorescent probe for measuring polymyxin-lipopolysaccharide binding interactions. *Anal Biochem* 409:273–283. <http://dx.doi.org/10.1016/j.ab.2010.10.033>.
 25. Azad MA, Yun B, Roberts KD, Nation RL, Thompson PE, Velkov T, Li J. 2014. Measuring polymyxin uptake by renal tubular cells: is BODIPY-polymyxin B an appropriate probe? *Antimicrob Agents Chemother* 58:6337–6338. <http://dx.doi.org/10.1128/AAC.03733-14>.
 26. Clinical and Laboratory Standards Institute. 2013. Performance standards for antimicrobial susceptibility testing: 23rd informational supplement, p 206. Clinical and Laboratory Standards Institute, Wayne, PA.
 27. Schneider CA, Rasband WS, Eliceiri KW. 2012. NIH Image to ImageJ: 25 years of image analysis. *Nat Methods* 9:671–675. <http://dx.doi.org/10.1038/nmeth.2089>.
 28. Garonzik SM, Li J, Thamlikitkul V, Paterson DL, Shoham S, Jacob J, Silveira FP, Forrest A, Nation RL. 2011. Population pharmacokinetics of colistin methanesulfonate and formed colistin in critically ill patients from a multicenter study provide dosing suggestions for various categories of patients. *Antimicrob Agents Chemother* 55:3284–3294. <http://dx.doi.org/10.1128/AAC.01733-10>.
 29. Velkov T, Roberts KD, Nation RL, Wang J, Thompson PE, Li J. 2014. Teaching ‘old’ polymyxins new tricks: new-generation lipopeptides targeting Gram-negative ‘superbugs’. *ACS Chem Biol* 16:1172–1177. <http://dx.doi.org/10.1021/cb500080r>.
 30. Azad MA, Atker J, Rogers KL, Nation RL, Velkov T, Li J. 2015. Major pathways of polymyxin-induced apoptosis in rat kidney proximal tubular cells. *Antimicrob Agents Chemother* 59:2136–2143. <http://dx.doi.org/10.1128/AAC.04869-14>.
 31. Malhotra JD, Kaufman RJ. 2011. ER stress and its functional link to mitochondria: role in cell survival and death. *Cold Spring Harb Perspect Biol* 3:a004424. <http://dx.doi.org/10.1101/cshperspect.a004424>.
 32. Dai C, Tang S, Deng S, Zhang S, Zhou Y, Velkov T, Li J, Xiao X. 2015. Lycopene attenuates colistin-induced nephrotoxicity in mice via activating the Nrf2/HO-1 pathway. *Antimicrob Agents Chemother* 59:579–585. <http://dx.doi.org/10.1128/AAC.03925-14>.